Preliminary Observations of the Type, Shape and Distribution of Inclusions Found in Submerged Arc Weldments

The distribution and structure of inclusions in a weldment are found to depend on the flux used and can determine toughness levels achieved

BY B. R. KEVILLE

ABSTRACT. A series of welds made under standard conditions with submerged arc fluxes have been examined, and a detailed description is given of the complex distribution, shape and composition of the inclusions found. It has been shown that the distribution and structure of inclusions in a weldment are dependent on the flux used and can determine the levels of toughness achieved.

Several examples are given showing how this information is currently being used to explain existing problems. Further work is still required to obtain a full understanding of the role of inclusions in weld metals.

Introduction

During a recent investigation into factors controlling the formation of hot cracks found in C-Mn steel weldments, much attention was paid to the examination and identification of weld metal inclusions; the reason for this was an initial feeling that specific types (*i.e.*, elongated inclusions) were the prime initiators (Ref. 1).

Further studies showed, however, that the cracking could be related to the different inclusion size distributions and the way in which these influenced the degree of pinning of prior austenite grain boundaries (Ref. 2) and not to specific inclusion types. Nevertheless, the detailed work carried out did highlight the different types, shapes and distributions of inclusions that could be found when welding with different types of fluxes; it was felt that a more extensive exercise should be carried out to determine whether nonmetallic inclusions in weld metals could be classified in any way.

This paper details the work carried out on inclusions in submerged arc welds made under standard conditions using several different fluxes and shows how specific problems may be related to inclusion morphology.

Experimental Procedure

A series of bead-on-plate welds were made on a 12.5 mm (0.49 in.) thick BS1501-224 type base metal (see Table 2) with a 1½% Mn filler metal electrode. Various fluxes were selected to cover the range of acid to basic and included:

Code	*Flux*	*Basicity*
A	OP170	0.37
B	SR2	0.36
C	BX200	1.1
D	OP41TT	3.7
E	BX300	4.2
F	OP121TT	3.3
G	Lincoln 3	0.72
H	ESAB 10:40	0.73

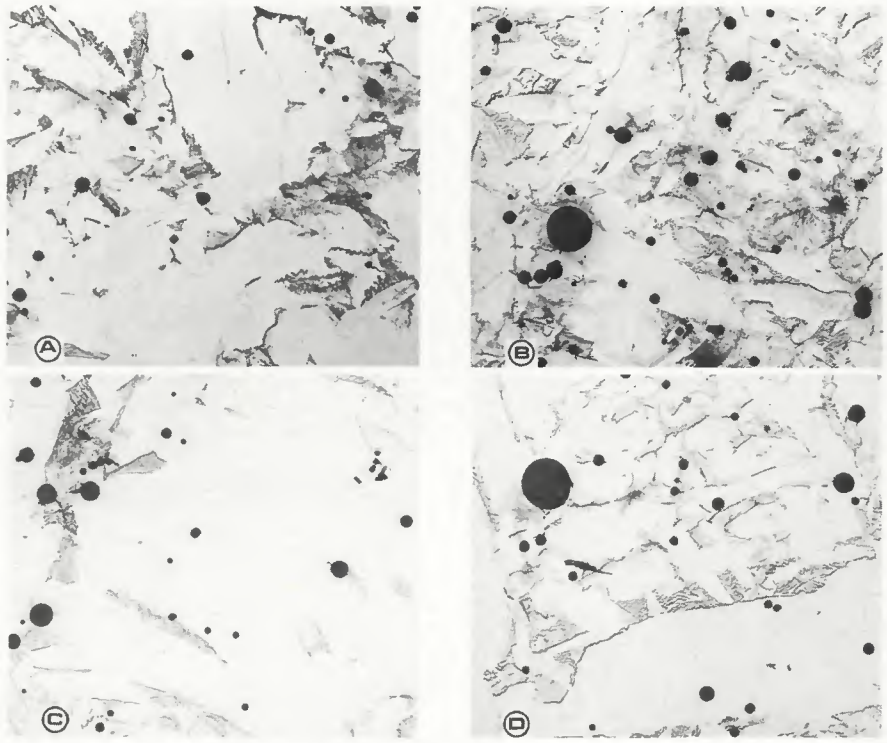

Fig. 1—Inclusion distribution for four fluxes: A—OP170 (code A flux); B—SR2 (code B flux); C—Lincoln 3 (code G flux); D—ESAB 1040 (code H flux). X1B00 (reduced 48% on reproduction)

B. R. KEVILLE is with Darchem Engineering Ltd., Stillington, England, and was Leading Welding Engineer, Welding Department, British Steel Corporation, Teeside Laboratories, Middlesbrough, England at the time the work discussed in this paper was performed.

Table 1—Flux Analyses, Wt-%

Flux designations		Flux constituents											
Code	Commercial	SiO_2	Al_2O_3	MgO	MnO	TiO_2	CaO	CaF_2	K_2O	Na_2O	Total FeO	Others	Basicity[a]
A	OP170	12.9	45.2	1.0	9.1	15.0	1.4	9.0	0.22	0.10	1.0	–	0.37
B	SR2	15.5	39.4	4.0	10.0	7.2	1.0	7.3	0.20	2.2	0.6	ZrO_2-13.0	0.36
C	BX200	18.0	31.2	18.0	8.0	1.5	9.0	4.88	0.20	1.2	2.06	ZrO_2-0.08	1.1
D	OP41TT	14.0	13.0	36.0	0.10	0.50	12.0	26.0	0.80	0.80	1.7	–	3.69
E	BX300	13.6	14.4	38.8	0.10	0.65	22.1	25.5	0.06	1.90	–	–	4.19
F	OP121TT	13.4	14.2	40.00	0.85	0.50	11.0	14.4	–	0.90	1.7	BaO[b] 0.10	3.26
G	Lincoln 3	44.8	4.5	4.1	34.8	0.20	7.7	3.9	–	0.10	1.1	–	0.72
H	ESAB 1040	43.9	4.0	5.7	35.5	0.1	9.2	–	0.10	0.10	1.4	Cr_2O_3-0.10; V_2O_3-0.10	0.73

(a) Basicity Index $= \frac{CaO + MgO + Na_2O + K_2O + CaF_2 + \frac{1}{2}MnO + FeO}{SiO_2 + \frac{1}{2}Al_2O_3 + \frac{1}{2}TiO_2 + \frac{1}{2}ZrO_2}$

(b) Compound form barium carbonate.

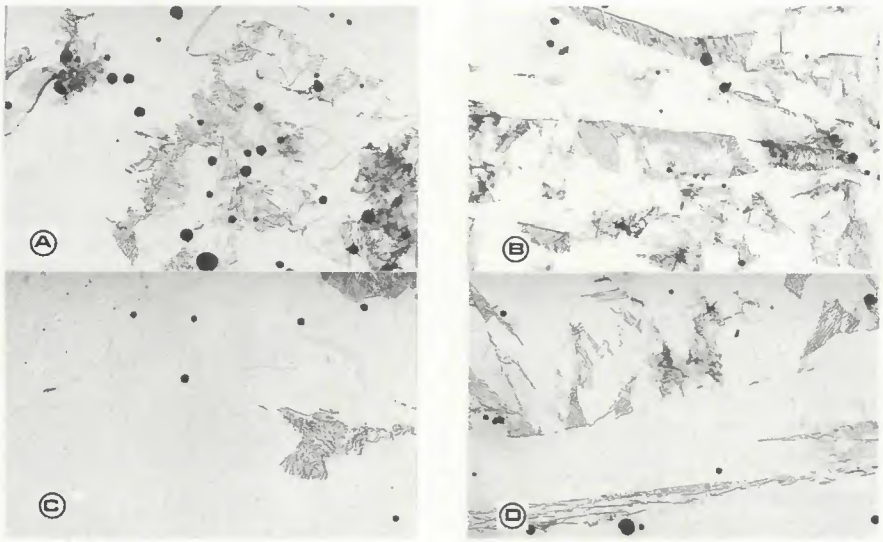

Fig. 2—Inclusion distribution for four additional fluxes: A—BX200 (code C flux); B—OP121TT (code F flux); C—BX300 flux (code E flux); D—OP41TT (code D flux). X1800 (reduced 48% on reproduction)

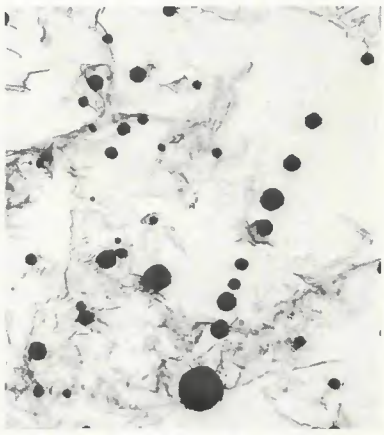

Fig. 3—Inclusions lining up along possible delta ferrite grain boundaries or solidification boundaries. Code C flux. X7200 (reduced 50% on reproduction)

Standard commercial fluxes were chosen, their full chemical analyses being given in Table 1; the resultant weld metal analyses are detailed in Table 2. Constant welding conditions were used throughout, and the conditions were: filler metal electrode diameter—4 mm (0.16 in.); voltage—35 A; current—620 A; forward welding travel—500 mm/min (19.7 ipm); heat input—2.5 kJ/mm (63.5 kJ/in.). To avoid inconsistencies, all the welds were made 100 mm (3.9 in.) long, and samples for metallographic examination and chemical analysis were extracted from either side of the mid point.

Samples were polished and examined under the optical microscope. However, no accurate assessment could be made of the inclusion type and morphology because of their finite size.

Detailed Electron Microscopy

Transmission and scanning electron microscope techniques were employed to assess the size, shape, distribution and composition of the inclusions in the weld metal using both solid samples and carbon extraction replicas.

Primarily, the investigation concentrated on the examination of carbon extraction replicas from the various welds, the objective being to catalogue the different types of inclusions found. This initial examination revealed the complex nature of the non-metallics present in weld metals and suggested that they may play a significant role in determining the levels of weld metal toughness

Table 2—Base and Weld Metal Analyses Obtained with Different Fluxes, Wt-%

Flux designation		Base/weld metal constituents											Total		
Code	Commercial	C	Si	Mn	P	S	Cr	Mo	Ni	Cu	Ti	Sn	Al	N_2	O_2
Base metal[a]		.18	.26	1.12	.014	.020	.040	–	–	.06	–	–	.06	–	–
A	OP170	.13	.28	1.15	.015	.019	.050	.010	.059	.059	.017	.005	.041	.0073	.052
B	SR2	.15	.33	1.19	.015	.019	.051	.011	.045	.065	.012	.006	.037	.0073	.060
C	BX200	.15	.21	1.12	.013	.014	.046	.009	.047	.057	–	.006	.033	.0075	.037
D	OP41TT	.15	.20	1.10	.014	.014	.047	.010	.046	.058	–	.005	.032	.0072	.020
E	BX300	.14	.25	1.28	.015	.018	.050	.011	.047	.061	–	.005	.032	.0074	.017
F	OP121TT	.15	.19	1.13	.014	.015	.049	.010	.047	.057	–	.005	.031	.0073	.021
G	Lincoln 3	.14	.45	1.30	.016	.017	.047	.010	.045	.073	–	.005	.024	.0074	.078
H	ESAB 1040	.14	.42	1.39	.016	.021	.045	.010	.045	.060	–	.018	.024	.0081	.092

(a) Balance—Fe.

Table 3—Inclusions Shapes with Key to Histograms of Figs. 7-14, 18 and 19

Histogram symbol[a]	Inclusion shape
O	Round
S	Complex (see Figs. 5B and 6)
Δ	Triangular (see Fig. 4B)
□	Square
E	Elongated (see Fig. 4A)
H	Hexagonal (see Fig. 5A)

(a) Located along abscissas (i.e., horizontal or x-axis) of histograms.

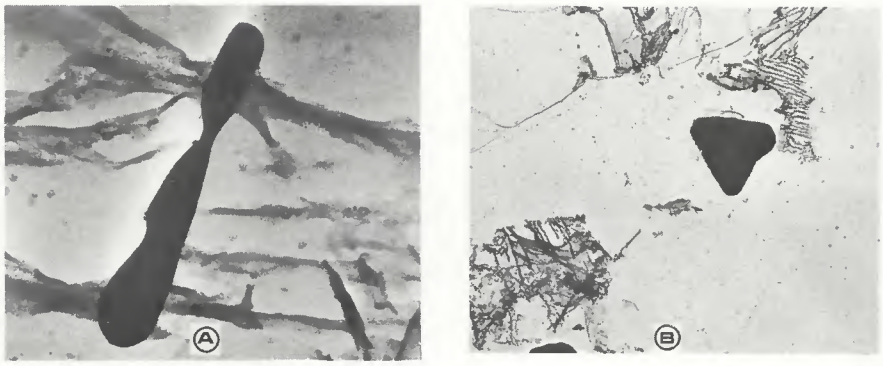

Fig. 4—Irregular shaped inclusions associated with: A—code H flux; B—code D flux. X11000 (reduced 50% on reproduction)

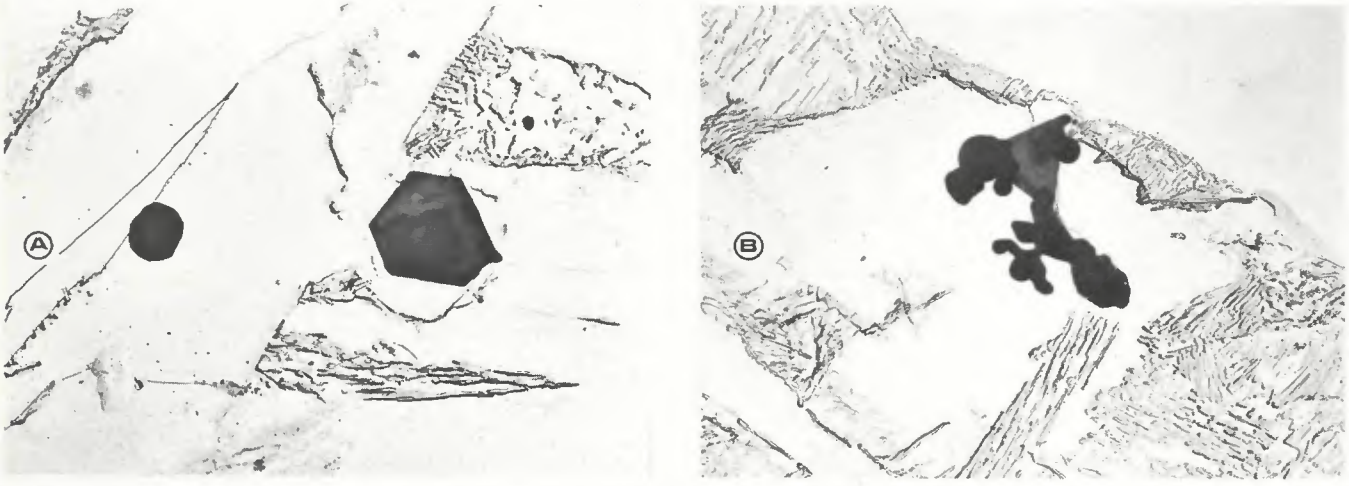

Fig. 5—Duplex nature of irregular shaped inclusions associated with: A—code C flux; B—code E flux. Magnifications as follows: A—X11000; B—X15000 (reduced 44% on reproduction)

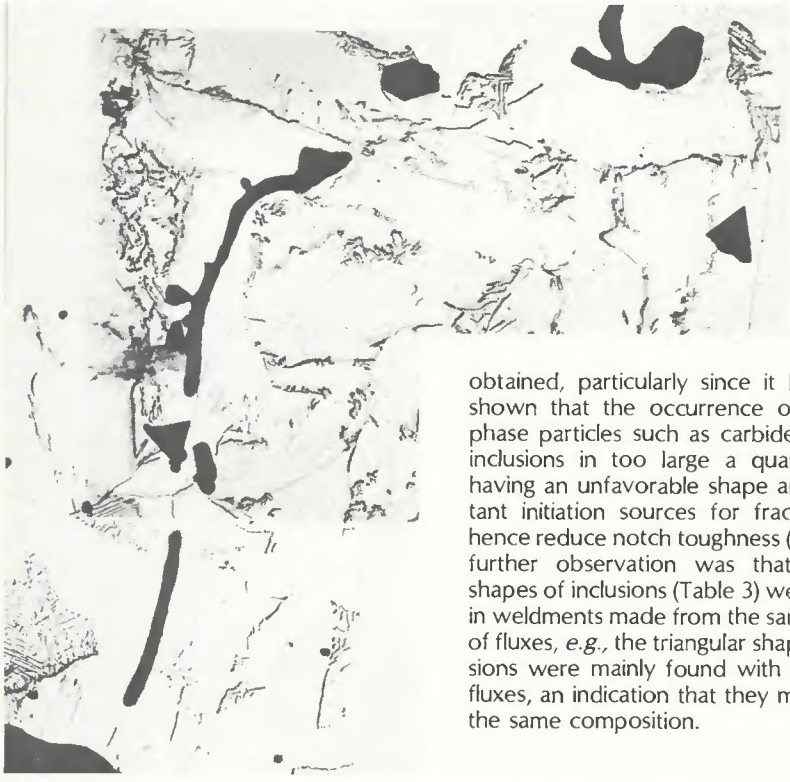

Fig.6—Complex shaped/duplex composition inclusions found in weldment made using code E flux

obtained, particularly since it has been shown that the occurrence of second phase particles such as carbides or slag inclusions in too large a quantity and having an unfavorable shape are important initiation sources for fracture and hence reduce notch toughness (Ref. 3). A further observation was that specific shapes of inclusions (Table 3) were found in weldments made from the same group of fluxes, *e.g.*, the triangular shaped inclusions were mainly found with the basic fluxes, an indication that they may be of the same composition.

Differences in the size and distribution of inclusions could be seen clearly when examining carbon extraction replicas on the transmission electron microscope. Figures 1 and 2 show typical areas from the various weldments, the density and size of inclusions being noticeably greater in the deposits from the acid and neutral fluxes (particularly fluxes H and G) than in the more basic E and D types as is generally expected. A further feature noted in the weldments of the acid/neutral fluxes was the way in which some inclusions lined up along what might well be delta ferrite or solidification boundaries (Fig. 3) instead of taking the more accepted random distribution in the matrix; this was most prevalent in the weld metal obtained using C flux.

In addition to the size and distribution variations between fluxes, certain weldments contained inclusions which had distinct geometric shapes, *i.e.*, triangles or hexagons in the case of welds made with fluxes D and C—Figs. 4B and 5A. Figure 5A clearly shows the duplex nature of the inclusion. Furthermore, evidence of more complex nonmetallics being formed in conjunction with these geometric shapes was found in several of the weldments, and in particular, flux E, as shown in Figs. 5B and 6.

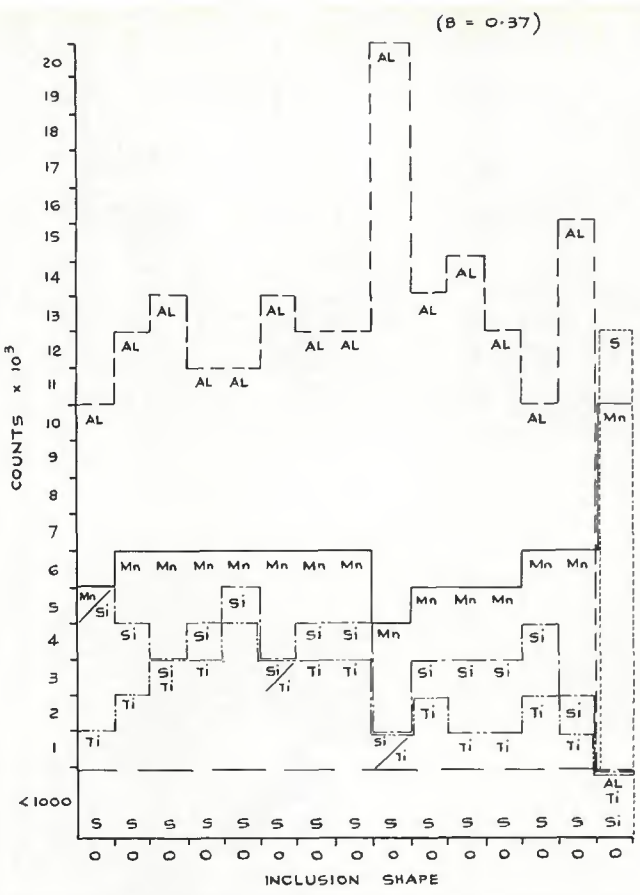

Fig. 7 (above)—Histogram of inclusion shapes associated with code A flux (see Table 3 for key to symbols)

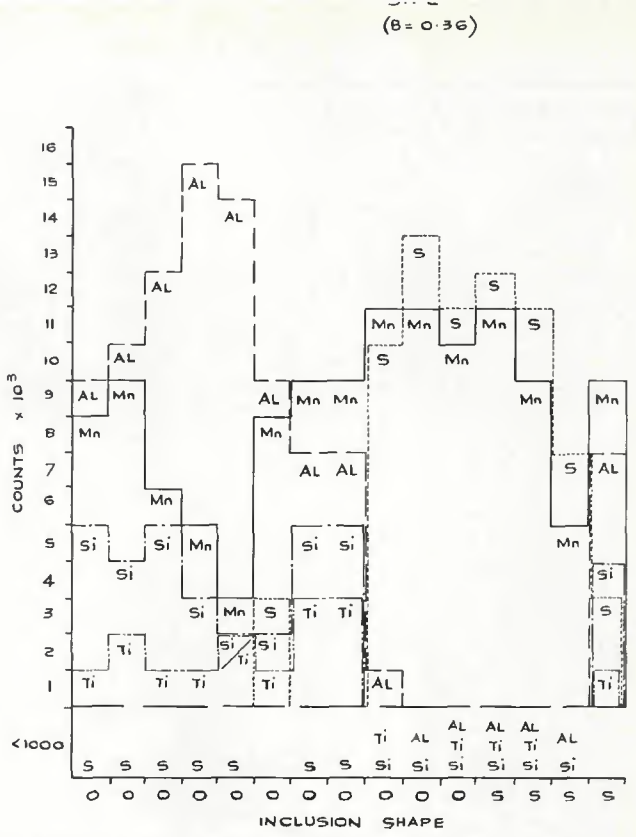

Fig. 8 (above)—Histogram of inclusion shapes associated with code B flux (see Table 3 for key to symbols)

Fig. 9 (below)—Histogram of inclusion shapes associated with code C flux (see Table 3 for key to symbols)

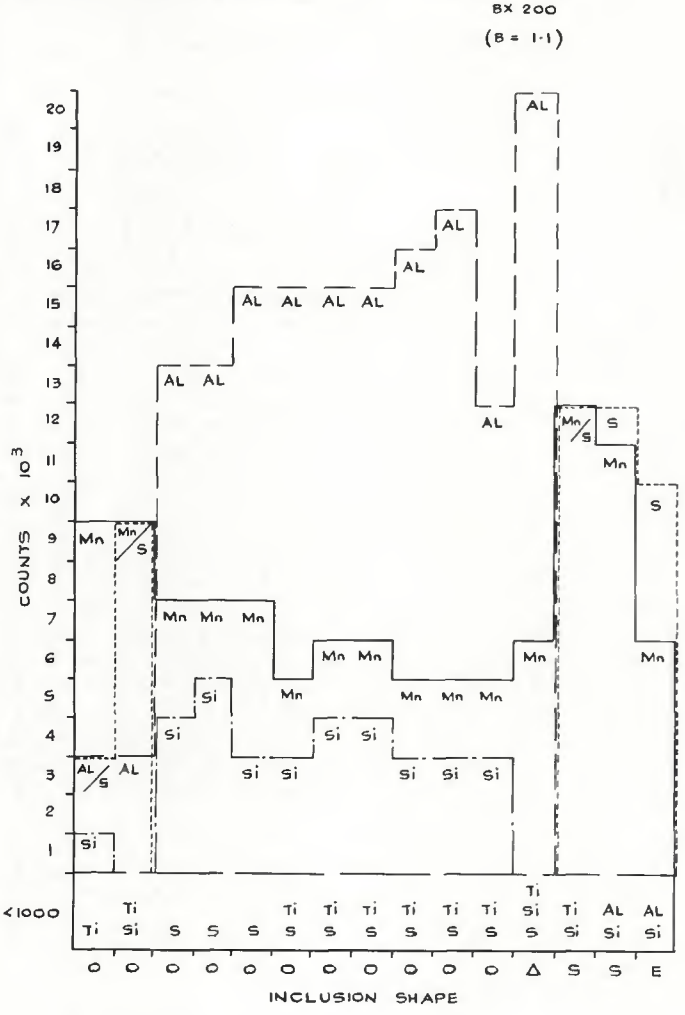

Fig. 10 (below)—Histogram of inclusion shapes associated with code D flux (see Table 3 for key to symbols)

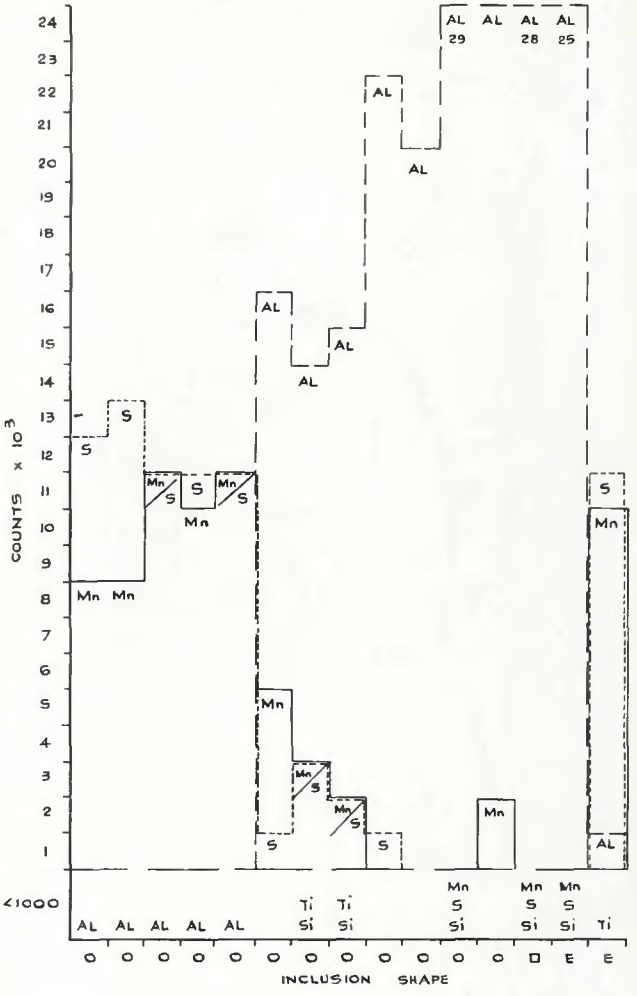

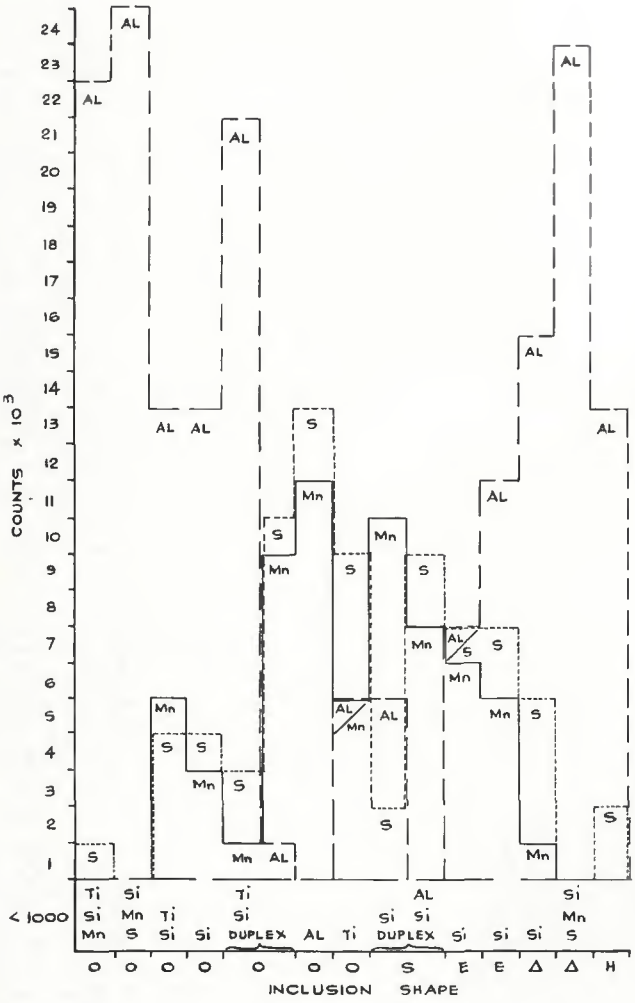

Fig. 11 (left) – Histogram of inclusion shapes associated with code E flux (see Table 3 for key to symbols)

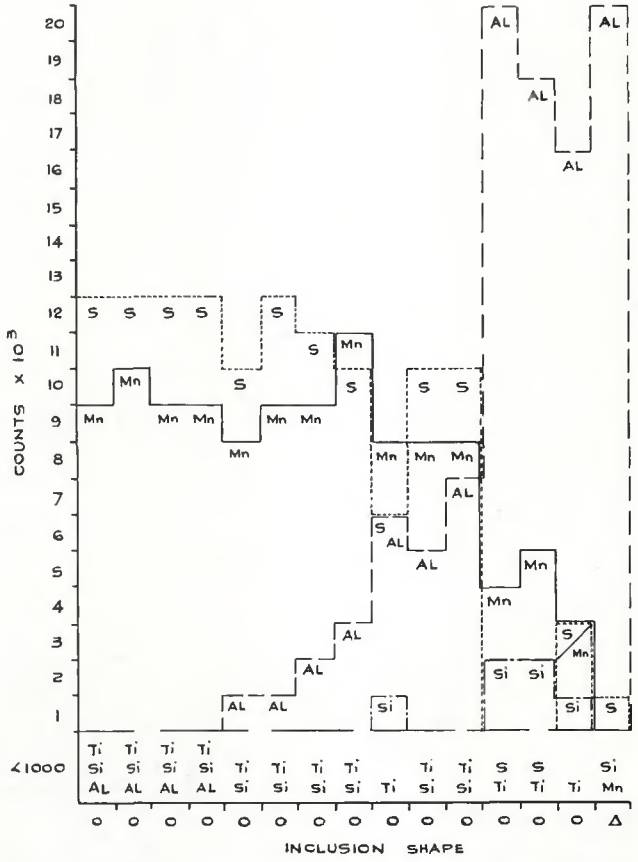

Fig. 12 (above) – Histogram of inclusion shapes associated with code F flux (see Table 3 for key to symbols)

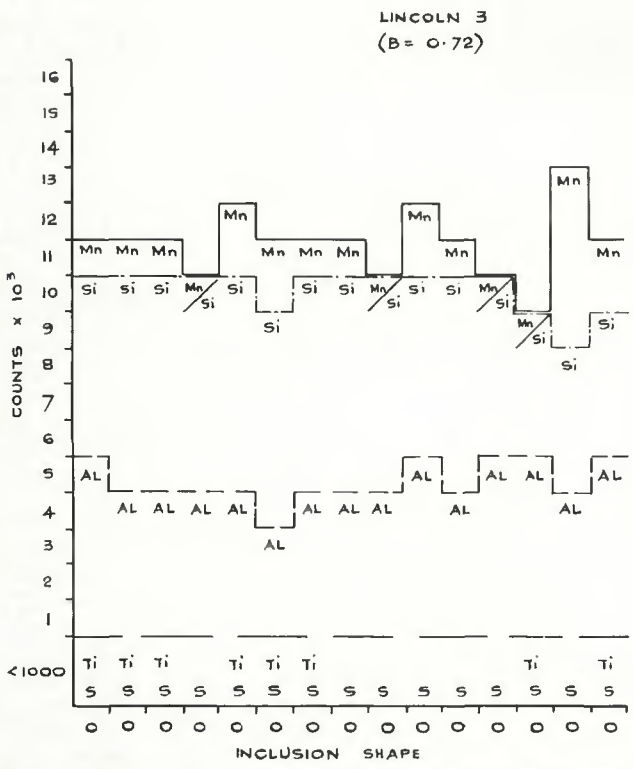

Fig. 13 – Histogram of inclusion shapes associated with code G flux (see Table 3 for key to symbols)

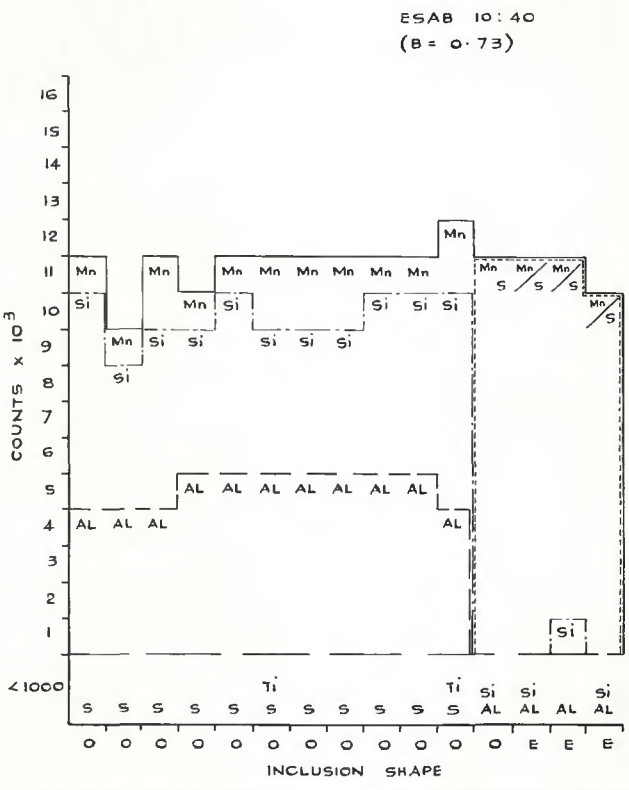

Fig. 14 – Histogram of inclusion shapes associated with code H flux (see Table 3 for key to symbols)

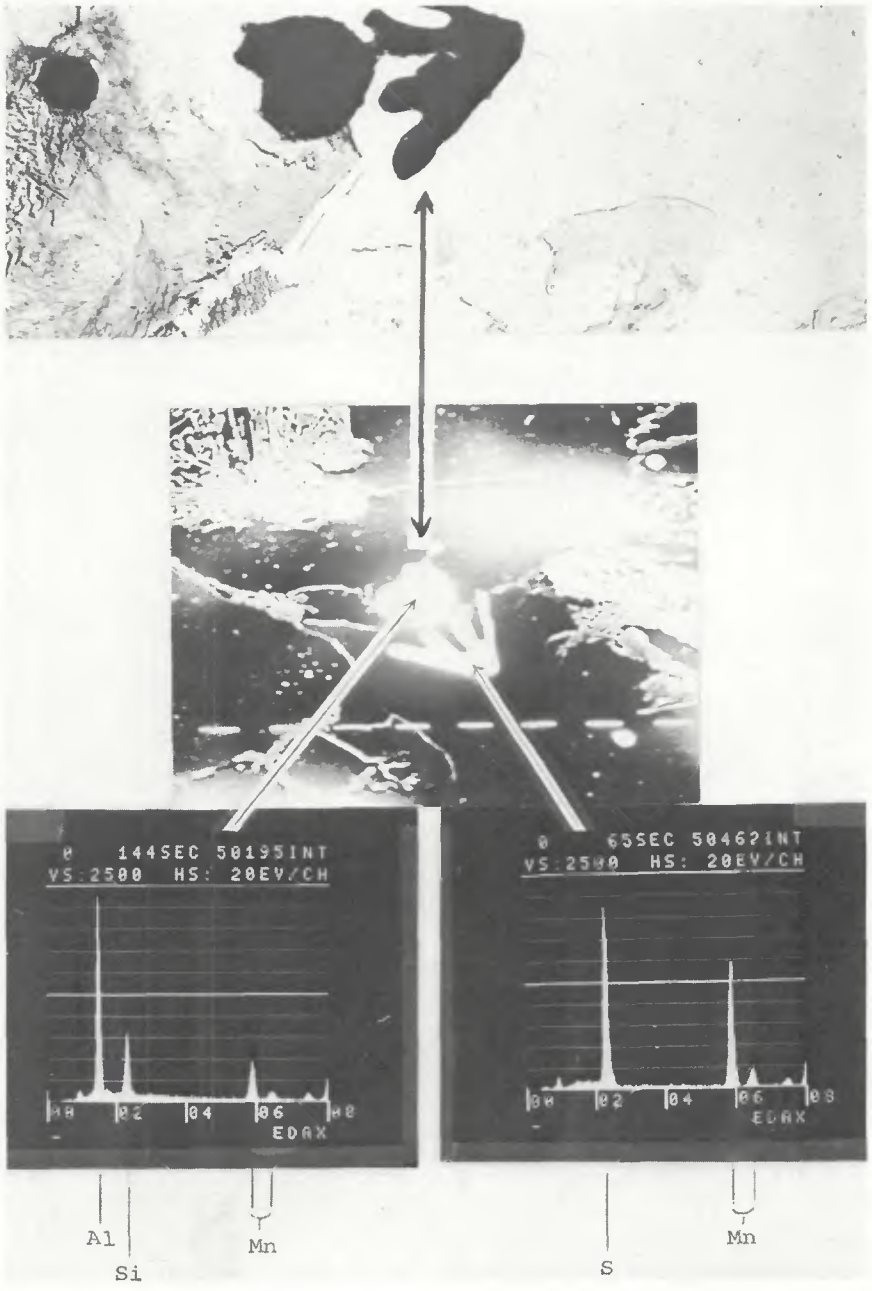

Fig. 15—TEM and SEM and EDAX analyses from a complex inclusion found in a weldment made using code E flux

Having shown that the size, distribution and shape of inclusions in a weldment can be related to the flux type, information was next required on any compositional variations that may exist between them. An extensive exercise was carried out using Philips scanning electron microscope (SEM) 500 with an X-ray energy dispersive analysis (EDAX) attachment involving random analysis of inclusions found on carbon extraction replicas. In total, 30 inclusions of varying shape and size per weld were examined and histograms representing the different analyses are given in Figs. 7–14.

Examination of the histograms shows clearly that a change in inclusion composition occurs from one flux to another, e.g., flux D consists mainly of Al_2O_3* type inclusions with some MnS, whereas flux H contains $MnO \cdot Al_2O_3 \cdot SiO_2$ type inclusions, again with some MnS. It follows that these differences can be related to the initial flux composition and hence deoxidation characteristics. The absence of MgO, a major constituent of flux D, from the inclusions may be noted and x-ray diffraction has shown that this compound is almost totally recovered in the welding slag (Ref. 4,5). Changes in inclusion shape have also shown analysis variations, *e.g.*, S and E inclusions of the type shown in Figs. 4A, 5B, and 6 are predominantly MnS; the triangular, hexagonal and square inclusions (Figs. 4B and 5A) are mainly Al_2O_3.

The large complex inclusions of the type shown in Figs. 5B and 6 were found to be duplex, *i.e.*, the round and/or triangular shapes being mainly Al_2O_3 and the adjoining film-like nonmetallic being Mn and S. Figure 15 shows an irregular shaped inclusion found on the TEM and SEM and the EDAX analysis obtained from it.

From this information it would appear that the shape and composition of inclusions in a weldment are a "fingerprint" of the flux used. Hence, with experience it should be possible to identify the particular flux without that prior knowledge. The identification of flux type (*i.e.*, acid or basic) is readily available from an examination of the weld metal microstructure. However, it is now thought that the actual flux (be it, for example, A or B) may be determined with the added information. A study of Figs. 7-14 will reveal that no two fluxes produce inclusions in the weld deposit with identical shapes and/or compositions.

Discussion

The complexity of both the shape, distribution and composition of nonmetallic inclusions in weld metals has been established. Hence, the next facet of this work was to determine whether any of this information could be used to relate fluxes and weldments with microstructure and properties.

It has already been suggested that inclusions in weld metals may influence significantly the rate of nucleation of ferrite, particularly from austenite grain boundaries. Consequently, the difference of microstructure and toughness that occurs between acid, amphoteric and basic deposits can be explained. Briefly the reasoning behind this inclusion hypothesis is twofold:

1. The austenite grain boundaries become pinned by oxide inclusions, thereby increasing the volume fraction of inclusion/grain boundary interface available for nucleation.

2. The inclusions themselves nucleate ferrite, and the extent of this is related to the volume fraction lying at the grain boundaries.

A more detailed explanation of this hypothesis can be found in a paper by Cochrane and Kirkwood (Ref. 6). What is very apparent is that the number, distribution and perhaps the shape of inclusions is very important when considering the role they play in nucleating ferrite. The distribution of inclusions as seen in Fig. 1 will strongly favor pinning the austenite grain boundaries, giving a fine grain of predominately side plate structures, *i.e.*, high temperature transforma-

**In all the examples of inclusion compositions used, other oxide constituents may also be present but only the major ones have been quoted, i.e., those giving >1000 counts.*

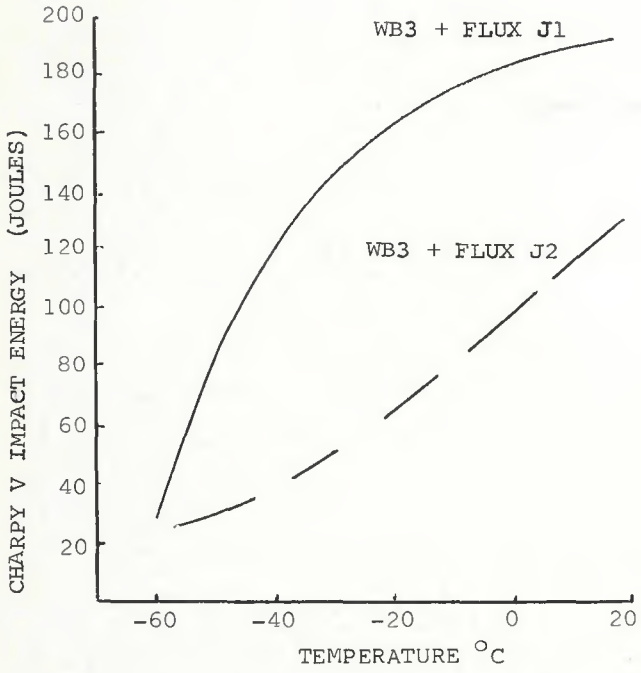

Fig. 16 — Variation in Charpy values obtained from weldments made with almost identical fluxes J1 and J2, all other variables being equal. Base material — 63 mm (2½ in.) thick BS4360 Grade 50D steel; welding preparation — 50 deg included angle, 5 mm (0.2 in.) root face; welding conditions — 800 A, 35 V, 254 mm/min (10 ipm) forward welding speed; heat input — 6.4 kJ/mm (163 kJ/in.); interpass control — 300°C (572°F). Chemical compositions (wt-%) as follows:

	J1	J2		J1	J2
SiO_2	14.0	13.6	CaO	12.0	22.1
Al_2O_3	13.0	14.4	CaF_2	26.0	25.5
MgO	36.0	38.8	K_2O	0.80	0.06
MnO	0.10	0.10	Na_2O	0.80	1.90
TiO_2	0.50	0.65	Basicity	3.69	4.19

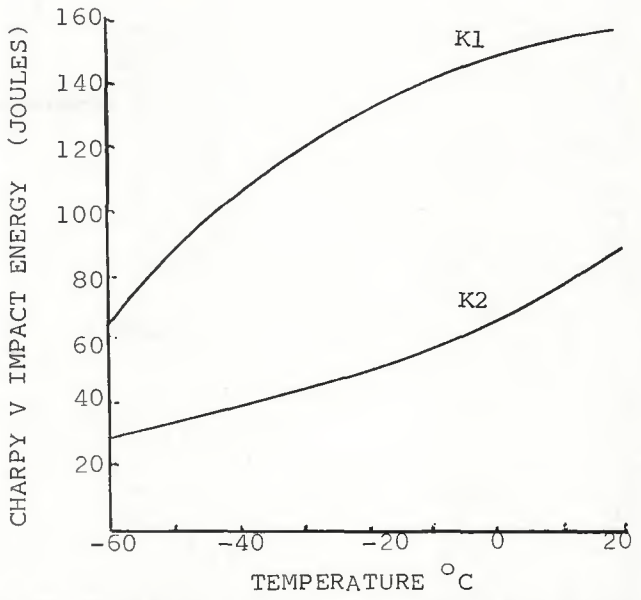

Fig. 17 — Variation in Charpy values obtained from weldments made with two additional almost identical fluxes K1 and K2, all other parameters being equal. Weld preparation — double-square groove with 8 mm (0.3 in.) root face; welding carried out on base material used for Fig. 16 at 1150 mm/min (45.3 ipm) forward welding speed using 4 mm (0.16 in.) diameter Mo-B-Ti steel filler metal electrodes. Current-voltage conditions as follows: side 1 — 750 A and 30 V (DC) on leading electrode, 650 A and 38V (AC) on trailing electrode; side 2 — 850 A and 30 V (DC) on leading electrode, 650 A and 38 V (AC) on trailing electrode. Chemical compositions (wt-%) as follows:

	K1	K2		K1	K2
SiO_2	14.1	13.6	K_2O	1.0	1.03
CaO	27.7	21.3	Na_2O	1.0	1.25
MgO	29.2	29.6	CaF_2	28.5	31.2
MnO	.53	.62	V_2O_5	.05	.05
Al_2O_3	17.1	22.5	Total Fe	.95	.60
TiO_2	.55	1.26	P_2O_5	.02	.03

tion structures. By contrast in the more basic deposits made using fluxes E and D (Fig. 2), fewer inclusions are present to pin the grain boundaries. Thus, a larger austenite grain size results, and the nucleation of high temperature transformation structures is suppressed in favor of intragranular plates.

It is widely accepted that the difference in inclusion volume fraction which determines, in part, the weld metal microstructure is a result of the deoxidation characteristics of the flux. However, what has not been considered is the influence their composition and shape may have on the rate of nucleation of ferrite and/or the structure of the ferrite formed.

The composition of the nonmetallics may be of prime importance, since variations in their surface energy would be expected to change the rate of nucleation. This effect has been demonstrated by Ohashi, *et al.* (Ref. 7), where the most potent inclusions for nucleating delta ferrite at temperatures close to the liquidus were found to be in descending order — REM oxides, Al_2O_3, SiO_2 and MnO. It is significant, therefore, that the basic/amphoteric deposits contain, primarily Al_2O_3 type inclusions, whereas the more acidic deposits contain $MnO \cdot Al_2O_3 \cdot SiO_2$ types. Hence it appears that the latter energetically favor the formation of Widmanstätten ferrite side plates in preference to the lower transformation products found more commonly in basic deposits. Furthermore, the shape of inclusions may be of importance when considering the match and mis-match that may exist between certain crystallographic planes in the inclusion and the ferrite; this will also be linked to compositional variations. More work is needed in this area to establish the true significance of the above observations.

A recent investigation involved the examination of weldments made with two very similar fluxes. It highlighted the important role of inclusions and their influence on weld metal microstructure and toughness. The two fluxes used had almost identical analyses, with the exception of CaO. However, when welded under the same conditions, they gave very different levels of toughness — Fig. 16. Examination of the weld metal microstructures revealed that J2 deposit was inferior to that of J1 deposit to an extent sufficient to explain the gross degredation in properties. Furthermore, when replicas from these welds were examined, large complex/elongated MnS type inclusions of the type shown in Figs. 6 and 15 were found in the weldment that had given the low Charpy energy levels.

The actual existence of the gross MnS inclusions (very similar to Type II sulphides found in base material) would in no way enhance the toughness of the weld metal and would be an obvious reason for seeing a reduction in the properties. Furthermore, it is felt that these nonmetallics could influence the rate of nucleation of ferrite in the matrix, hence resulting in a poor microstructure. However, the mechanism behind the formation of the gross nonmetallics is not understood in detail. It is suggested that it is primarily related to the rate of deoxidation of the weld metal and, secondarily, to the overall cooling rate of the weld pool.

Variations in inclusion composition have been found in weldments, which can usually be related to the flux type. However, during an evaluation of some alternative fluxes proposed for use with

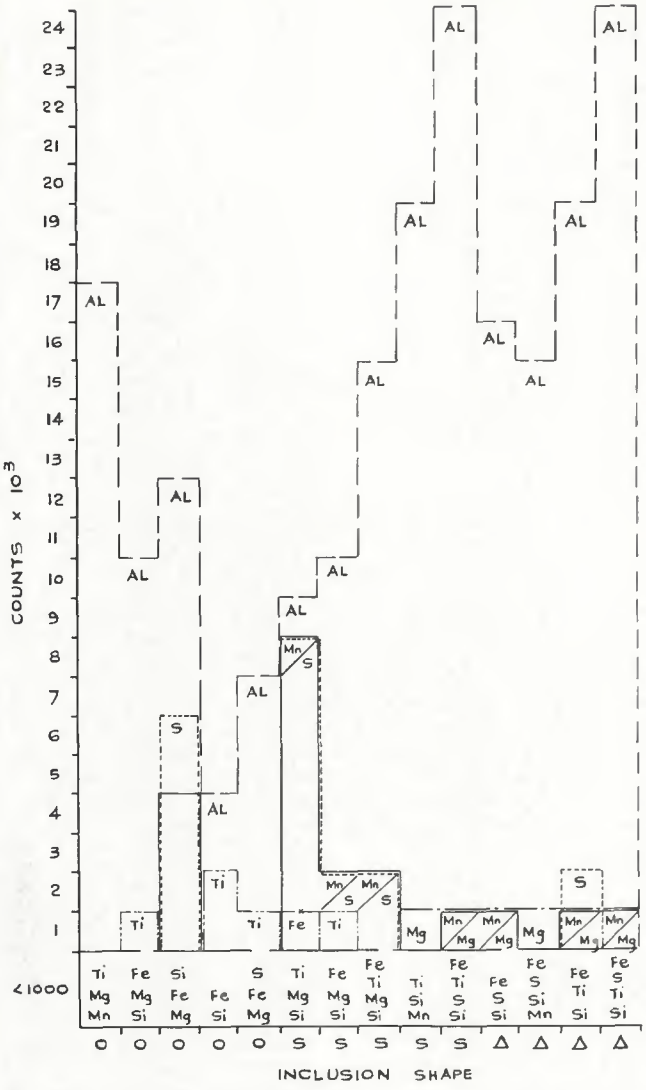

Fig. 18—Histogram of inclusion shapes associated with K1 flux (see Table 3 for key to symbols)

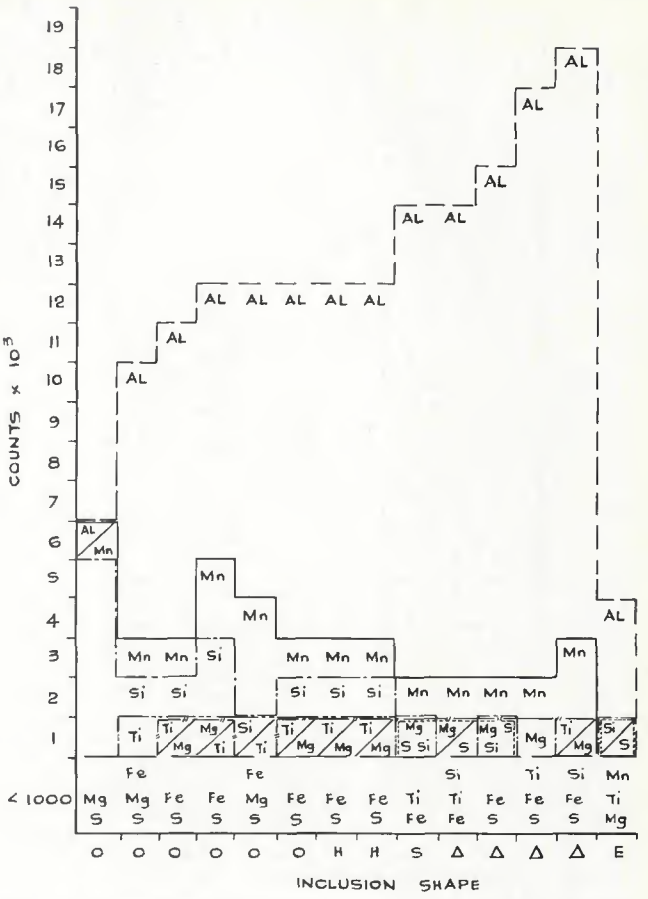

Fig. 19—Histogram of inclusion shapes associated with K2 flux (see Table 3 for key to symbols)

the Mo-B-Ti submerged arc filler metal electrode (Ref. 8), it was noted that two fluxes of almost identical analyses gave deposits with different levels of toughness and inclusions of different composition—Fig. 17.

Microstructurally, the weldments were found to be almost identical, the poorer deposit having marginally more polygonal ferrite but not sufficient to have caused the dramatic reduction in weld metal toughness. TEM examination of the carbon extraction replicas did not reveal any distinct variation in inclusion distribution. However, it was clear that differences existed between the compositions of inclusions in weld A when compared to those in weld B—Figs. 18 and 19.

The weld made with K1 was found to have inclusions containing mainly Al_2O_3 with small amounts of MnO, MgO · TiO_2 and S, and hence was very refractory in nature. By comparison, the weld made with K2, having the increased level of toughness, contained less refractory inclusions; although Al_2O_3 was the major constituent, increased amounts of MnO and SiO were also present together with TiO_2, MgO and S. This information tends to suggest that the deoxidation characteristics of the seemingly similar fluxes are, in fact, quite different and that the resultant inclusions are influencing the properties of the weld metal. Work is continuing in this area to establish the cause of the large variation in properties with such a small change in flux composition.

The topics discussed here are just a few examples of how basic knowledge of the complexity of inclusions in weld metals can be used. Many questions still remain unanswered. It is clear from the studies carried out to date that further detailed investigations are required before a full understanding of inclusions, their distributions and structures can be obtained.

Conclusions

The complexity of distribution, shape and composition of inclusions in weldments has been established. These are a "fingerprint" of the flux used and hence it should be possible to identify the exact flux used without that prior knowledge. Examples are given of how specific problems have been related to inclusion distribution and structure. Further work is still required before a full understanding of inclusions, their distributions and structures can be obtained.

Acknowledgment

The author wishes to thank the British Steel Corporation for permission to publish this paper.

References

1. Cochrane, R. C., *et al.* Private communication.

2. Cochrane, R. C., and Keville, B. R. 1978. Strain induced hot cracking in ferritic weld metals. Paper presented at Welding Institute international conference, November 14-16 1978.

3. ISI and BSC (British Steel Corp.). 1971. Proceedings of conference on effect of second phase particles on the mechanical properties of steel. Scarborough.

4. Butler, S. A. Private communication *a*

5. Butler, S. A. Private communication *b*

6. Cochrane, R. C., and Kirkwood, P. R. 1978. The effect of oxygen on weld metal microstructure. Paper presented at Welding Institute conference on trends in steels and consumables for welding, November 13-16 1978, London.

7. Ohashi, T., *et al.* 1977. Effects of oxides on nucleation behaviour in supercooled iron. *Iron and Steel Inst. Japan* 17(5):262-271.

8. Kirkwood, R. P. Private communication.